# Pharmacological targeting of netrin-1 inhibits EMT in cancer

Justine Lengrand, Ievgenia Pastushenko, Sebastiaan Vanuytven, Yura Song, David Venet, Rahul Sarate, Melanie Bellina, Virginie Moers, Alice Boinet, Alejandro Sifrim, et al.

# Pharmacological targeting Netrin-1 inhibits EMT in cancer

Justine Lengrand[1,2,3]*, Ievgenia Pastushenko[1]*, Sebastiaan Vanuytven[4,5,]*, Yura Song[1], David Venet[6], Rahul M. Sarate[1], Melanie Bellina[2,3], Virginie Moers[1], Alice Boinet[1], Alejandro Sifrim[5,7], Nicolas Rama[3], Benjamin Ducarouge[2], Jens Van Herck[4], Christine Dubois[1], Samuel Scozzaro[1], Sophie Lemaire[1], Sarah Gieskes[1], Sophie Bonni[1], Amandine Collin[8,9], Nicolas Braissand[2,3], Justine Allard[8,9], Egor Zindy[8,9], Christine Decaestecker[8,9,10], Christos Sotiriou[6], Isabelle Salmon[8,9,11], Patrick Mehlen[2,3], Thierry Voet[4,7], Agnès Bernet[2,3] , Cédric Blanpain[1,12]

[1]Laboratory of Stem Cells and Cancer, Université Libre de Bruxelles (ULB), Brussels, Belgium

[2]NETRIS Pharma, Lyon, France

[3]Laboratory Apoptosis, Cancer and Development, Equipe labellisee 'La Ligue', LabEx DEVweCAN, Institute PLAsCAN, Centre de Recherche en Cancérologie de Lyon, INSERM U1052-CNRS UMR5286, Université Lyon 1, Centre Léon Bérard, Lyon, France.

[4]Department of Human Genetics, University of Leuven, KU Leuven, Leuven, Belgium

[5]Laboratory of Multi-omic Integrative Bioinformatics, Center for Human Genetics, KU Leuven, 3000, Leuven, Belgium

[6]Laboratory of Breast Cancer Translational Research J.-C. Heuson, Institut Jules Bordet, Hôpital Universitaire de Bruxelles (H.U.B), Université Libre de Bruxelles (ULB), 1000 Brussels, Belgium

[7]KU Leuven Institute for Single-cell Omics, KU Leuven, Leuven, Belgium[7]Institut Jules Bordet, Hopital Universitaire de Bruxelles (HUB), Brussels, Belgium

[8]Centre Universitaire Inter Régional d'Expertise en Anatomie pathologique Hospitalière (CurePath), Jumet, Belgium

[9]DIAPath, Center for microscopy and molecular Imaging, Université Libre de Bruxelles (ULB), Gosselies, Belgium

[10]Laboratory of Image Synthesis and Analysis, Ecole Polytechnique-Université libre de Bruxelles (EPB-ULB), Brussels, Belgium

[11]Departement of Pathology, Erasme University Hospital, Université Libre de Bruxelles (ULB), Brussels, Belgium

[12]Walloon Excellence in Life Sciences and Biotechnology (WELBIO), Université Libre de Bruxelles (ULB), Brussels, Belgium

*Indicates co-first authors

Correspondences: cedric.blanpain@ulb.be, patrick.mehlen@lyon.unicancer.fr and agnes.bernet@lyon.unicancer.fr

**Epithelial-to-Mesenchymal transition (EMT) regulates tumour initiation, progression, metastasis and resistance to anti-cancer therapy[1-7]. Whereas great progress had recently been made in understanding the role and mechanisms that regulate EMT in cancer, no therapeutic strategy to pharmacologically target EMT had been identified so far. Here, we found that Netrin-1 is upregulated in a primary mouse model of skin squamous cell carcinoma (SCCs) presenting spontaneous EMT. Pharmacological inhibition of Netrin-1 by administrating NP137, an anti-Netrin-1 blocking monoclonal antibody currently used in clinical trials in human cancer[8], decreased the proportion EMT tumour cells in skin SCCs, as well as decreased the number of metastasis and increased the sensitivity of tumour cells to chemotherapy. Single-cell RNA-seq revealed the presence of different EMT states including epithelial, early and late hybrid EMT as well as fully EMT states in control SCCs. In contrast, administration of NP137 prevents the progression of cancer cells towards a late EMT state and sustains tumour epithelial states. ShRNA knockdown (KD) of Netrin-1 and its receptor Unc5b in EPCAM+ tumour cells inhibited EMT *in vitro* in the absence of stromal cells and regulated a common gene signature promoting tumour epithelial state and restricting EMT. To assess the relevance of these findings to human cancers, we treated mice transplanted with A549 human cancer cell line that undergoes EMT following TGF-β1 administration[9,10] with NP137. Netrin-1 inhibition decreased EMT in A549 cells *in vivo*. Altogether, our results identify a new pharmacological strategy to target EMT in cancer opening novel therapeutic interventions for anti-cancer therapy.**

## Introduction

Epithelial-to-Mesenchymal Transition (EMT) in which tumour cells (TCs) lose their epithelial characteristics and acquire mesenchymal features, is a key driver of tumour heterogeneity and has been associated with tumour initiation, progression, metastasis and resistance to chemotherapy or immunotherapy[2,4-7,11,12]. Whereas great progress in the understanding of the role and the mechanisms by which EMT regulates these different cancer features has been achieved, there is still very little non-genetic pharmacological interventions that allow to inhibit EMT in primary tumours, decrease their metastatic potential or potentiate the response to anti-cancer therapy.

## Netrin-1 is expressed in EMT skin SCC

To identify novel therapeutic strategies that can inhibit EMT, we searched in RNA-sequencing from epithelial and mesenchymal TCs isolated from a skin squamous cell carcinoma (SCC) model that presented spontaneous EMT (*Lgr5CREER/KRasG12D/p53cKO/Rosa-YFP or LKPR*)[13-15] for secreted factors preferentially expressed by mesenchymal EPCAM- TCs compared to epithelial EPCAM+ TCs and for which specific therapy targeting this factor was available and currently administrated to cancer patients. We found that *Netrin-1* and its receptor *Unc5b* were overexpressed in EPCAM- EMT TCs as compared to EPCAM+ epithelial TCs (Fig. 1a, b). Netrin-1 has been shown to regulate tumour progression in multiple cancer models by preventing apoptosis of TCs, promoting neo-angiogenesis and controlling the pro-tumorigenic cancer associated fibroblast function[16-27]. The therapeutic anti-Netrin-1 blocking antibody NP137 is currently tested in clinical trial for the treatment of cancer patients[8].

**Netrin-1 overexpression increases EMT**

To assess Netrin-1 promotes EMT, we first overexpressed human NETRIN-1 in LKPR mouse (*Lgr5CREER/KRasG12D/p53cKO/Rosa-YFP/Rosa-NETRIN-1*) (Extended data 1a-c). Following NETRIN-1 overexpression, there was an increase in the number of tumours per mouse (Fig. 1c) and the proportion of TCs that underwent EMT as compared to control mice (Fig. 1d, Extended data 1d).As previously reported, EMT is not a binary process and occurs in a step wise manner through the presence of intermediate states of EMT[3,6,7,15,28-30]. We have thus assessed by histological analysis and by immunofluorescence the impact of NETRIN-1 overexpression on the different tumour states including epithelial (KRT14+/VIM-), hybrid EMT (KRT14+/VIM+) and late EMT (KRT14-/VIM+) previously described in this model[15]. Immunostaining revealed that control skin SCCs were heterogeneous and 20% of them were epithelial (KRT14+/VIM-), 35% presented hybrid EMT (KRT14+/ VIM+) and 45% had full EMT (KRT14-/VIM+) (Fig. 1e, f). By contrast, overexpression of NETRIN-1 led to a significant increase in tumours with full EMT (70%) and a decrease of SCCs with epithelial phenotype (3%) (Fig. 1e, f), in good accordance with the EPCAM expression quantified by FACS (Fig. 1d). These data demonstrate that overexpression of NETRIN-1 promotes tumour initiation and EMT in a primary model of skin SCC.

**Targeting Netrin-1 inhibits EMT**

Although previous studies reported *in vitro* an upregulation of Netrin-1 occurring in several cancers presenting EMT [31-34], the effect of pharmacological inhibition of Netrin-1 on EMT *in vivo* has not been investigated so far. To assess whether the pharmacological inhibition of Netrin-1 inhibits EMT, we administrated an anti-Netrin-1 blocking monoclonal antibody (NP137) to LKPR mice 4 weeks following Tamoxifen administration and determined the impact of Netrin-1 inhibition on tumour formation and EMT (Extended data 1e). NP137

administration three times per week led to a decrease of 50% in the number of SCCs per mouse (Fig. 1g). FACS quantification of the percentage of YFP+/EPCAM+ TCs (i.e., epithelial cells) and YFP+/EPCAM- TCs (i.e. cells that underwent EMT) showed that NP137 administration decreased the proportion of EPCAM- TCs that underwent EMT (41% in NP137-treated vs 77% in control mice) in primary skin SCCs presenting spontaneous EMT, showing that in the LKPR mouse model, pharmacological targeting of Netrin-1 inhibits EMT (Fig. 1h). To determine whether Netrin-1 inhibition differentially affects the different EMT states, we assessed by immunofluorescence the proportions of tumours states. NP137 administration increased the proportion of epithelial state (54% in NP137-treated vs 31% in the control mice), whereas the proportion of hybrid EMT was unchanged (16% in NP137-treated vs 12% % in the control mice) and the proportion of late EMT state was decreased (30% in NP137-treated vs 56% in the control mice) (Fig. 1i, j). These data demonstrate that pharmacological targeting of Netrin-1 inhibits EMT in primary mouse model of cancer.

**Targeting Netrin-1 inhibits metastasis**

EMT has been shown to play an important role for metastasis formation in different mouse models and is associated with resistance to anti-cancer therapy[1,4-6,11,12,35]. We first assessed whether pharmacological inhibition of Netrin-1 in LKPR mice decreased primary metastasis formation. NP137 administration strongly decreased the number of lung metastasis in LKPR mice (Fig. 2a), suggesting that Netrin-1 is important for the formation of spontaneous lung metastasis. As the number of tumours was reduced in LKPR mice treated with NP137, it is possible that the reduction of the number of lung metastases was the consequence of the reduced number of tumours. To clarify this issue, we injected YFP+ TCs intravenously and assessed the number of lung metastases upon pharmacological Netrin-1 inhibition. NP137 administration strongly decreased the number of lung metastases following tail vein injection

of FACS isolated YFP+ TCs from LKPR mice, demonstrating that Netrin-1 inhibition directly inhibits metastasis formation (Fig. 2b).

**NP137 sensitizes cancer cells to chemotherapy**

EMT has been shown to promote resistance to chemotherapy in skin SCCs[2,36]. To assess whether pharmacological targeting of Netrin-1 can sensitize TCs to chemotherapy, we administrated Cisplatin/5-Fluoracil (5-FU), a standard chemotherapy for the treatment of human SCCs[37,38] and assessed the impact of Netrin-1 inhibition on the response to chemotherapy. The combination of NP137 with Cisplatin/5-FU significantly potentiated the effect of Cisplatin/5-FU on the inhibition of tumour growth in primary SCCs from LKPR mice (Fig. 2c). These data demonstrate that pharmacological targeting of Netrin-1 can decrease the cancer features associated with EMT including metastasis and resistance to therapy.

**Effect of NP137 on stromal cells**

To assess in a comprehensive manner the impact of Netrin-1 inhibition on the different EMT tumour states and the composition of the tumour stroma, we performed single-cell RNA-sequencing (10x Genomics Chromium) of TCs and their associated stromal cells in 2 control and 2 NP137-treated primary skin SCCs. Unsupervised clustering revealed the presence of different cell populations in primary skin SCCs (Extended data 2), including TCs identified by *Yfp* and expression and *Epcam* (Extended data 3a, b), immune cells (marked by CD45/*Ptprc* expression), combined each other with CD86 for myeloid cells, *Cxcr2* for neutrophils or *Cd3d* for lymphocytes T cells), cancer associated fibroblasts (CAFs, expressing *Acta2* and *Pdgfra* and negative for *Yfp*), and endothelial cells (expressing *Pecam1*) (Extended data 3c, d). This clustering reveals that *Ntn1* is expressed in EMT TCs and CAFs in skin SCC from LKPR presenting spontaneous EMT (Extended data 3e).

158 After integration of the tumour of the tumour microenvironment across the conditions, we
159 observed that NP137 administration decreased the proportion of TCs and changed the
160 composition of the tumour stroma, with a relative increase in the proportion of CAFs (Extended
161 data 4a-d). Using scCODA to perform differential abundance analysis, we found no significant
162 difference in the proportion of the different CAF clusters (3 myCAFs, 2 iCAFs, proliferative
163 and glycolysis CAFs) or gene expression within these clusters between the two control and two
164 NP137-treated mice (Extended data 4e-h). Immunostaining analyses confirmed the relative
165 increase of CAFs following NP137 administration (Extended data 4i).
166
167 **Impact of NP137 on tumour cell states**
168 To assess more specifically the impact of Netrin-1 inhibition on the tumour states, we
169 clustered at higher resolution the YFP+ TCs of control and NP137-treated mice (Fig. 3a, b). In
170 the control tumour, different clusters corresponding to distinct EMT cell states ranging from
171 epithelial (*Epcam*+/*Krt14*+/*Vim*-), early hybrid EMT (*Epcam*-/*Krt14*+/*Vim*+), late hybrid EMT
172 (*Epcam*-/*Krt14*-/*Krt8*+/*Vim*+/*Pdgfra*-), and late EMT (*Epcam*-/*Krt14*-, *Krt8*-/*Vim*+/*Pdgfra*+)
173 were identified (Fig. 3a, Extended data 5a). NP137 administration was associated with an
174 increase in the proportion of epithelial TC state, a similar proportion of early, a decreased
175 proportion of late hybrid EMT and a strong decrease in the late EMT as compared to control
176 (Fig. 3b, c, Extended data 5b, c). *In situ* immunofluorescence for KRT14, VIM, KRT8 and
177 PGFRA confirmed the increase of epithelial states and the decrease of the late EMT tumour
178 state upon NP137 administration (Fig. 3d).
179
180 Spatial transcriptomic analysis using Visium 10x unravelled the spatial localization of
181 the different tumour states identified by single-cell RNA-seq and showed that they were
182 localised in distinct niches as previously reported[15]. NP137 administration increased the

epithelial state (*Epcam*+/*Krt14*+) and inhibited the occurrence of late EMT state (*Krt14*-/*Krt8*-/*Vim*+) blocking EMT progression at the hybrid EMT state (*Krt8*+/*Vim*+) (Fig. 3e, f, Extended data 6).

To further understand the mechanisms and signalling pathways by which NP137 administration regulates EMT, we have performed pathway analyses using the MSigDB Hallmark genesets[39] on the single-cell RNA-seq data. These analyses revealed that pathways associated with EMT, hypoxia, angiogenesis and inflammatory response were all significantly decreased in TCs following Netrin-1 inhibition (Fig. 3g).

Lineage trajectory analysis revealed that two distinct lineage trajectories could be identified in the control tumour, with a trajectory going from epithelial cells towards hybrid EMT and another trajectory going from the epithelial state toward the late full EMT state (Fig. 4a). NP137-treated tumour cells were characterized by different lineage trajectories with the absence of a trajectory toward the late EMT state expressing high level of *Aqp1* and the appearance of two new trajectories toward epithelial states (Epithelial-B1 and Epithelial-B2), and two different hybrid EMT trajectories (Fig. 4b). Epithelial-B1, was characterized by high expression of *Krt15*, while gene ontology (GO) terms enrichment analysis of marker genes of cells belonging to Epithelial-B2 revealed an upregulation of glycolysis and a higher keratinization (Fig. 4b, c).

*In situ* analysis using RNA-fish and Visium 10x spatial transcriptomic on tumour sections of control and NP137-treated tumours showed a decrease of *Aqp1* expressing cells (Fig. 4d) and an increase of TCs expressing *Krt15* following Netrin-1 inhibition confirming the inhibition of the late EMT trajectory and the increase of epithelial states upon NP137 administration (Fig. 4e). Altogether these data reveal that EMT is characterized by the presence

of different EMT tumour states with two different differentiation trajectories of epithelial state toward distinct EMT states and that the pharmacological targeting of Netrin-1 inhibits the switch of epithelial into the late EMT state and promotes tumour cell differentiation into epithelial state.

**Netrin-1/Unc5b axis promotes EMT**

Netrin-1 has been proposed to play a pleiotropic role in cancer including a cellular autonomous role in tumour proliferation and apoptosis as well as a non-cellular autonomous mechanism regulating tumour growth by controlling tumour angiogenesis and CAFs functions [16-27]. Our single-cell analysis shows that NP137 administration modulates the composition of the tumour microenvironment and the proportion of the different EMT tumour cell states. NP137 has been shown to specifically inhibit the interaction of Netrin-1 with its receptor Unc5b[40]. To assess whether the regulation of EMT and the promotion of pro-epithelial states by NP137 administration is the consequence of a disruption of a paracrine or an autocrine Netrin-1/Unc5b signalling axis that directly regulates EMT states, we studied the impact of genetic knockdown (KD) of *Netrin-1* and *Unc5b* on EMT states in a tumour cell autonomous manner *in vitro* in the absence of the tumour microenvironment. FACS isolated EPCAM+ TCs from primary SCCs from LKPR mice and cultured *in vitro* progressively underwent EMT as shown by the progressive loss of EPCAM expression by TCs (Fig. 5a) with an average of 60% of EPCAM+ TCs that switch to EPCAM- TCs over 2 weeks in culture. Interestingly, both ShRNA KD of *Netrin-1* and *Unc5b*, resulted in a strong decrease of the ability of EPCAM+ TCs to switch to the EPCAM- EMT phenotype (Fig. 5a). The inhibition of EMT upon ShRNA KD of *Netrin-1* and *Unc5b* was accompanied by a decrease in cell migration that was not further enhanced by NP137 administration (Fig. 5b).

To assess the molecular mechanisms by which Netrin-1 and Unc5b signalling regulate EMT, we performed bulk RNA-seq of EPCAM+ TCs from control, *Netrin-1* KD, and *Unc5b* KD TCs cultured *in vitro* 6 days after plating of FACS isolated Epcam+ TCs. We found that more than 50% of the genes downregulated and upregulated following *Unc5b* KD were also differentially regulated by *Netrin-1* KD (Fig. 5c), showing that Netrin-1 and Unc5b regulate a similar signalling pathway and transcriptional program. Consistent with the results of the single-cell RNA-seq following NP137 administration, *Netrin-1* and *Unc5b* KD promote the expression of genes associated with the epithelial state (eg: *Krt14*, *Krt15*, *Involucrin*, *Claudin*) (Fig. 5d) and decrease the expression of genes associated with EMT and promoting EMT (eg: *Aqp5*, *Nrp1*, *Nr2f2*, *Twist1*, *Twist2*) (Fig. 5e-g). Altogether, these data demonstrate that targeting Netrin-1/Unc5b signalling axis in TCs decrease EMT and promote epithelial state in skin SCCs in a cellular autonomous manner independently of the tumour microenvironment.

**NP137 prevents EMT in human cancer**

To assess the human and clinical relevance of our findings, we first assessed the correlations between Netrin-1 expression, Unc5b expression and EMT signature in human non-small cell lung carcinoma (lung SCC and lung adenocarcinoma) and melanoma. We used several human EMT signature previously described[12,39,41] and the gene expression dataset from the panTCGA version of lung SCC (LUSCC) (484 primary tumors), lung adenocarcinoma (LUAD) (510 primary tumors) and skin cutaneous melanoma (SKCM) (76 primary tumors, 367 metastasis). While Netrin1 expression was not strongly associated with the EMT score, there was a very good correlation between the expression of Netrin1 receptor Unc5b and the different EMT scores in these 3 cancers (Fig 6a, b).

To assess the functional relevance of these data, we then assessed the impact of blocking Netrin-1/Unc5b signaling on EMT in A549 human lung adenocarcinoma cell line, the most

commonly used human cancer cell line that can undergo EMT in a plastic manner upon TGF-β1 administration[9,10]. A549 cells were treated with recombinant TGF-β1 *in vitro* for 3 days, which promoted mesenchymal cell morphology, increased Netrin-1 expression and promoted EMT as shown by the upregulation of Vimentin and downregulation of E-cadherin expression (Fig. 6c, d). We next performed subcutaneous grafting of these A549 cells that underwent EMT cells into immunodeficient mice and administrated anti-Netrin-1 antibody every two days. Interestingly, immunostaining analysis revealed that Netrin-1 inhibition significantly increases the number of TCs expressing high levels of epithelial marker E-cadherin (Fig. 6e, f), demonstrating that Netrin-1 inhibition decreases EMT in human cancer cells in vivo. Treatment of a human endometrial adenocarcinoma cell line (Ishikawa cells) with NP137 following their transplantation into immunodeficient mice decreased tumour growth (Extended data 7a) and resulted in an increase in epithelial gene expression (Extended data 7b), further demonstrating that targeting Netrin1 inhibits EMT. Consistent with the decrease of EMT induced by Netrin1 inhibition, we found that NP137 administration decreased cell migration *in vitro* (Extended data 7c).

**Discussion**

Our study demonstrates that pharmacological targeting of Netrin-1 using NP137, an anti-Netrin-1 blocking monoclonal antibody currently tested in phase II clinical trials for the treatment of different solid tumours is a safe and effective strategy to target EMT in primary mouse and human tumours, decreasing lung metastasis and increasing the response of tumour cells to chemotherapy.

Our bioinformatics analysis of single-cell RNA-seq data upon Netrin-1 inhibition combined with *in situ* characterization revealed the molecular mechanisms by which Netrin-1 regulates EMT and promotes a late EMT differentiation trajectory. Inhibition of Netrin-1

induces a switch in the lineage differentiation of tumour cells that redirect the tumour differentiation toward an epithelial tumour state that is more sensitive to chemotherapy and less prone to give rise to metastasis. Netrin-1 exerts its pro-EMT function by signalling to Unc5b, which regulates positively the expression of a mesenchymal transcriptional program and negatively the expression of genes controlling cell-cell adhesion and promoting the epithelial differentiation program. The sensitization of tumour cells to chemotherapy following NP137 administration suggests that the combination of anti-Netrin-1 antibody with might be beneficial for patients with cancer presenting EMT features.

We also demonstrated the human relevance of pharmacological targeting EMT following treatment with anti-Netrin-1 blocking antibody in human lung cancer cell line and endometrial adenocarcinoma that presents EMT plasticity, demonstrating that pharmacological inhibition of EMT can be achieved in human cancers *in vivo* in pre-clinical settings.

Altogether, our study provides the proof of principle that pharmacological targeting of EMT in primary mouse tumour model and human cancers is now possible. These results have important implications for developing new strategies for anti-cancer therapy combining Netrin-1 inhibition in patients with cancer presenting EMT, for the development of novel biomarkers that will help to better stratify the cancer patients that are more likely to respond to anti-Netrin-1 therapy.

## ACKNOWLEDGMENTS

We thank ULB animal facility, ULB genomic core facility (Frederick Libert and Anne Lefort) for bulk RNA-sequencing and single-cell sequencing, the Gilles Thomas bioinformatic plateform, Centre de Recherche en Cancérologie de Lyon, Fondation Synergie Lyon cancer for the spatial transcriptomic sequencing and Sophie Bottieau (DIAPath, CMMI) for her technical assistance. We thank Fabrice Lavial for kindly providing *Unc5b* ShRNA. We thank Rik Derynck for kindly providing A549 cell line. J.L. is supported by NETRIS Pharma. I.P. is supported by FNRS and WELBIO. S.V. is supported by a PhD fellowship for Strategic Basic Research (1S93320N) from the Research Foundation Flanders (FWO). C. Decaestecker is a senior Research Associate with the "Fond National de la Recherche Scientifique" (FNRS, Brussels, Belgium). DIAPath and the department of pathology are supported by the Fonds Yvonne Boël. The CMMI is supported by the European Regional Development Fund and the Walloon region. C.B. is supported by WELBIO, FNRS, TELEVIE, Fondation Contre le Cancer, ULB Foundation, Foundation Baillet Latour, FNRS/FWO EOS (40007513) and the European Research Council (AdvGrant 885093).

## AUTHOR CONTRIBUTION

J.L., I.P., S.V. and C.B. designed the experiments and performed data analysis. J.L. and I.P. performed most of biological experiments. S.V. performed most of bioinformatic analysis for single-cell sequencing. N.R., Y.S. and A.S. helped for bioinformatic analysis. J.V.H. helped with 10x single-cell sequencing. R.M.S. helped with RNA-Scope analysis. V.M., A.B., S.S., S.L., S.G. and S.B. helped with cell culture experiments immunostainings, blocking antibody injection and follow-up of the mice. I.S., J.A., E.Z, C.D. and A.C. performed immunostaining and quantification of EMT in human cancer samples. B.D., M.B and N.B performed biological *in vivo* and *in vitro* experiments on Ishikawa endometrial cell lines. C.S and D.V. performed

bioanalysis from TCGA. C.D. performed FACS sorting. T.V. helped and supervised the single-cell data analysis. P.M. and A.B. helped with the design of the experiments, data analysis and provided NP137 antibody. All authors read and approved the final manuscript.

## COMPETING INTERESTS

Authors declare potential competing interests.

J.L., P.M. A.B., B.D., M.B and N.B are employees of NETRIS Pharma, Lyon, France.

T.V. is co-inventor on licensed patents WO/2011/157846 (Methods for haplotyping single cells); WO/2014/053664 (High-throughput genotyping by sequencing low amounts of genetic material); WO/2015/028576 (Haplotyping and copy number typing using polymorphic variant allelic frequencies).

## DATA AVAILABILITY STATEMENT

All raw data sequencing data for mouse RNA-seq, single cell RNA-seq and 10x Visium have been deposited in the gene expression Omnibus with the following accession number: GSE234267

## FIGURE LEGENDS

**Figure 1. Targeting Netrin-1 inhibits EMT. a**, **b**, Relative mRNA expression of *Ntn1* (**a**) and *Unc5b* (**b**) in EPCAM+ (n= 4) as compared to EPCAM- (n= 10) tumour cells (TCs) defined by qRT-PCR (data are normalized to *Tbp* gene, mean ± s.e.m., two-tailed Mann-Whitney U test). **c**, Dot plot showing the number of tumours in control (n= 16) and NETRIN-1 gain of function (n= 17) mice (mean ± s.e.m., two-tailed t test). **d**, Proportion of EPCAM+ TCs in control (n= 34 tumours from n= 16 mice) and NETRIN-1 gain of function mice (n= 70 tumours from n= 17 mice) (mean ± s.e.m., two-tailed t test). **e**, Co-immunostaining of YFP and KRT14 or Vimentin in primary control and NETRIN-1 gain of function tumours (n= 21 tumours from 11 control mice and n= 34 tumours from 9 NETRIN-1 gain of function mice) (Scale bars, 20 μm). **f**, Percentage of tumours presenting epithelial (KRT14+/VIM-), hybrid EMT (KRT14+ and VIM+) and full EMT (KRT14-/VIM+) (n= 21 tumours from n= 11 control mice and n= 34 tumours from n= 9 NETRIN-1 gain of function mice). **g**, Dot plot showing the number of tumours in control (n= 10) and NP137 treated (n= 15) mice (mean ± s.e.m., two-tailed t test). **h**, Proportion of EPCAM+ TCs in control (n= 148 tumours from n= 20 mice) and NP137 -treated (n= 117 tumours from 16 mice) skin SCC mice (mean ± s.e.m., two-tailed t test). **i**, Co-immunostaining of YFP and KRT14 or Vimentin in control and NP137-treated skin SCC (n= 32 tumours from 10 control mice and n= 24 NP137 treated SCCs from 9 mice) (Scale bars, 20 μm). **j**, Percentage of tumours presenting epithelial (KRT14+/VIM-), hybrid EMT (KRT14+ and VIM+) and full EMT (KRT14-/VIM+) (n= 32 tumours from 10 control mice and n= 24 NP137-treated SCCs from 9 mice).

**Figure 2. Targeting Netrin-1 reduces metastasis and sensitizes tumour cells to chemotherapy in skin SCC. a**, Dot plot showing the number of spontaneous lung metastases

in control (n= 12) and NP137-treated (n= 11) mice presenting skin SCC (mean ± s.e.m, two-tailed t test). **b**, Dot plot showing the number of lung metastases arising from the intravenous injection of 1000 EPCAM- TCs (n= 18 mice injected control mice and n= 18 mice injected for NP137-treatment) (mean ± s.e.m, two-tailed t test). **c,** Relative tumour volume overtime of control tumours (n= 29 from 5 mice) or upon therapy with Cisplatin/5-Fluoracil (5-FU) (n= 58 from 8 mice), anti-Netrin-1 antibody (n= 29 from 5 mice) or combination of Cisplatin/5-FU and anti-Netrin-1 (n= 59 from 8 mice) (mean + s.e.m., two-tailed t test). Tumour volumes were normalized to the tumour volume at the 1$^{st}$ day of chemotherapy.

**Figure 3. Pharmacological inhibition of Netrin-1 inhibits late EMT and promotes epithelial tumour states. a**, **b,** Uniform Manifold Approximation and Projection **(**UMAP) plots coloured by the EMT states for control (**a**) and NP137-treated YFP+ TCs skin SCC (**b**). The colours represent the different tumour states. **c,** Boxplot depicting the proportion of the different tumour states for the 4 samples in control and NP137-treated conditions. The centre line, top and bottom of the boxplots represent respectively the median, 25th and 75th percentile and whiskers are 1.5 × IQR. Significant proportion changes are indicated by FDR < 0.2**. d,** Co-immunostaining of YFP and KRT14, KRT8, Vimentin or PDGFRA in control (left) and anti-Netrin-1 treated skin SCC (right) that define areas with different degrees of EMT (n= 3 control tumours, n= 3 NP137-treated tumours) (Scale bars, 20 µm). **e**, Spatial transcriptomic using 10x VISIUM was conducted on tumour sections of control and NP137-treated mice. Normalized gene expression values are visually represented as a colour gradient. **f**, Summary of the different areas presenting different tumour states based on the expression of *Epcam*, *Krt14*, *Krt8* and *Vim* (green area highlights epithelial state: *Epcam+/Krt14+/Vim-*; orange area highlights early hybrid EMT state: *Epcam-/Krt14+/Vim+*; red area defines late hybrid EMT state: *Epcam-/Krt14-/Krt8+/Vim+*; dark red defines late full EMT state: *Epcam-/Krt14-/Krt8-/Vim+*). **g,**

Combined boxplot and violin plot displaying the activity of 4 MSigDB[37] hallmark gene sets (Epithelial-to-Mesenchymal Transition, Hypoxia, Angiogenesis and Inflammatory response) in control (n=2) and NP137-treated (n=2) tumours. The "Area Under the Curve" (AUC) value depicts whether the different hallmark gene sets are enriched between control and NP137 treated tumours (the center line, top and bottom of the boxplots represent respectively the median, 25$^{th}$ and 75$^{th}$ percentile and whiskers are 1.5 × the interquartile range (IQR), two-sided Wilcoxon rank-sum test with Bonferroni correction).

**Figure 4. Pharmacological inhibition of Netrin-1 inhibits late EMT promotes epithelial differentiation trajectories of tumour cells. a, b,** Pseudotemporal analysis using Monocle2 showing lineage trajectories in control skin SCC showing two EMT trajectories (hybrid and full EMT trajectories) (**a**) and in NP137-treated skin SCC showing the absence of the late EMT trajectory and the appearance of new epithelial trajectories (**b**). Dots represent single cells. Green , orange, red and dark red colors respectively represent the epithelial state, the early hybrid, the late hybrid EMT and the late EMT state. Gene expression is visualized as a colour gradient with blue indicating no expression and red indicating maximum expression. Two new branches were detected in the NP137-treated trajectory, indicated by Epithelial-B1 and Epithelial-B2. **c**, Combined boxplot and violin plot displaying the activity of glycolysis and keratinization gene sets for the TCs belonging to the new epithelial state and other EMT states based on GO terms analysis in NP137-treated tumours (n=2) (the centre line, top and bottom of the boxplots represent respectively the median, 25$^{th}$ and 75$^{th}$ percentile and whiskers are 1.5 × IQR, two-sided Wilcoxon rank-sum test with Bonferroni correction). **d,** Immunostaining for YFP and RNA in situ hybridization (RNA-scope) for *Krt14*, *Vim,* or *Aqp1* in control and NP137-treated skin SCCs (n = 2 independent biological replicates , Scale bars, 20 μm). **e**, *Krt15* expression spots using 10x VISIUM spatial transcriptomic on tumour sections. Gene expression

values have been normalized in the control and treated sample and are visualized as colour gradient (scale bars, 500 μm).

**Figure 5. Netrin-1 and Unc5b knockdown inhibits EMT and promotes epithelial state. a,** EPCAM expression following *in vitro* culture of FACS isolated primary EPCAM+ tumour cells transduced with empty vector, *Ntn1* and *Unc5b* ShRNA KD (n= 8 independent replicates for empty vector, n= 6 independent replicates for *Unc5b* KD and n= 3 independent replicates for *Ntn1* KD; mean ± s.e.m., two-tailed t test) **b**, Percentage of migrated Epcam – LKPR cells quantified with crystal violet staining (n=2 independent replicates, 3 wells per condition; mean± s.e.m, two-tailed Mann-Whitney U test). **c**, Venn diagram showing the overlap between the genes upregulated and downregulated in *Ntn1* and *Unc5b* KD cell lines. **d**, mRNA expression of upregulated epithelial genes as defined by RNA-sequencing of EPCAM+ cells 6 days after plating of 100% EPCAM + TCs (Histograms represent mean, n= 2 for empty vector, *Ntn1* KD and *Unc5b* KD). **e**, mRNA expression of mesenchymal genes downregulated upon *Ntn1* KD and *Unc5b* KD, as defined by RNA-sequencing in EPCAM+ cells 6 days after plating of 100% EPCAM+ TCs (Histograms represent mean, n= 2). **f, g**, *In situ* hybridization (RNA-scope) for *Nrp1* (**f**) and *Aqp5* (**g**) in empty vector control, *Ntn1* and *Unc5B* KD cell line. (n = 2 independent biological replicates, Scale bars, 20 μm).

**Figure 6. Anti-Netrin-1 therapy inhibits EMT in human cancer cells. a,** Scatterplots of *NTN1* and *UNC5B* expression versus Hallmark EMT signatures are shown across Lung squamous cell carcinoma (LUSCC) (n= 484 primary tumors), and Lung adenocarcinoma (LUAD) (n= 510 primary tumors) cancer types from TCGA, one dataset per row. Spearman correlations are shown in each panel top left corner. **b**, Barplots with Spearman correlations between *NTN1*, *UNC5B* expression and three EMT signatures[12,39,41] are shown across lung SCC

(LUSCC) (n = 484 primary tumors), lung adenocarcinoma (LUAD) (n = 510 primary tumors), and skin cutaneous melanoma (SKCM) (n = 443 tumors including 76 primary tumors and 367 metastases) cancer types from TCGA, as well as 95% confidence intervals (eventually clipped at 0 for low correlations). **c,** Microscopic appearance of A549 NSCLC cell line not treated or after 3 days upon TGF-β1 treatment (n = 3, scale bars, 20 μm). **d,** Western blot analysis of Netrin-1, E-cadherin and Vimentin expression in human A549 NSCLC cell line in control conditions or following 3 days of TGF-β1 treatment. **e,** Co-immunostaining of E-cadherin and Pan-cytokeratin on tumours arising from subcutaneous grafting into immunodeficient mice of A549 NSCLC cell line pre-treated with TGF-b1 *in vitro* for 6 days. The mice were treated with physiologic serum or NP137 for 25 days and the tumours were collected for histological analysis (scale bars, 20 μm) **f**, Percentage of Pan-cytokeratin + TCs expressing high levels of epithelial marker E-cadherin in tumours (each dot represents the mean of CDH1 high cells in 4 representative areas from each tumour, n= 6 control tumours and n= 6 NP137 treated tumours) (mean ± s.e.m., two-tailed t test).

## References


1 Ye, X. & Weinberg, R. A. Epithelial-Mesenchymal Plasticity: A Central Regulator of Cancer Progression. *Trends Cell Biol* **25**, 675-686, doi:10.1016/j.tcb.2015.07.012 (2015).

2 Shibue, T. & Weinberg, R. A. EMT, CSCs, and drug resistance: the mechanistic link and clinical implications. *Nat Rev Clin Oncol* **14**, 611-629, doi:10.1038/nrclinonc.2017.44 (2017).

3 Lambert, A. W. & Weinberg, R. A. Linking EMT programmes to normal and neoplastic epithelial stem cells. *Nat Rev Cancer* **21**, 325-338, doi:10.1038/s41568-021-00332-6 (2021).

4 Puisieux, A., Brabletz, T. & Caramel, J. Oncogenic roles of EMT-inducing transcription factors. *Nat Cell Biol* **16**, 488-494, doi:10.1038/ncb2976 (2014).

5 Brabletz, S., Schuhwerk, H., Brabletz, T. & Stemmler, M. P. Dynamic EMT: a multi-tool for tumor progression. *EMBO J* **40**, e108647, doi:10.15252/embj.2021108647 (2021).

6 Pastushenko, I. & Blanpain, C. EMT Transition States during Tumor Progression and Metastasis. *Trends Cell Biol* **29**, 212-226, doi:10.1016/j.tcb.2018.12.001 (2019).

7 Nieto, M. A., Huang, R. Y., Jackson, R. A. & Thiery, J. P. Emt: 2016. *Cell* **166**, 21-45, doi:10.1016/j.cell.2016.06.028 (2016).

8 https://clinicaltrials.gov/ct2/show/NCT02977195.

9 Kasai, H., Allen, J. T., Mason, R. M., Kamimura, T. & Zhang, Z. TGF-beta1 induces human alveolar epithelial to mesenchymal cell transition (EMT). *Respir Res* **6**, 56, doi:10.1186/1465-9921-6-56 (2005).

10 Kim, J. H. *et al.* Transforming growth factor beta1 induces epithelial-to-mesenchymal transition of A549 cells. *J Korean Med Sci* **22**, 898-904, doi:10.3346/jkms.2007.22.5.898 (2007).

11 Voon, D. C., Huang, R. Y., Jackson, R. A. & Thiery, J. P. The EMT spectrum and therapeutic opportunities. *Mol Oncol* **11**, 878-891, doi:10.1002/1878-0261.12082 (2017).

12 Tan, T. Z. *et al.* Epithelial-mesenchymal transition spectrum quantification and its efficacy in deciphering survival and drug responses of cancer patients. *EMBO Mol Med* **6**, 1279-1293, doi:10.15252/emmm.201404208 (2014).

13 Lapouge, G. *et al.* Skin squamous cell carcinoma propagating cells increase with tumour progression and invasiveness. *EMBO J* **31**, 4563-4575, doi:10.1038/emboj.2012.312 (2012).

14 Latil, M. *et al.* Cell-Type-Specific Chromatin States Differentially Prime Squamous Cell Carcinoma Tumor-Initiating Cells for Epithelial to Mesenchymal Transition. *Cell Stem Cell* **20**, 191-204 e195, doi:10.1016/j.stem.2016.10.018 (2017).

15 Pastushenko, I. *et al.* Identification of the tumour transition states occurring during EMT. *Nature* **556**, 463-468, doi:10.1038/s41586-018-0040-3 (2018).

16 Paradisi, A. *et al.* Combining chemotherapeutic agents and netrin-1 interference potentiates cancer cell death. *EMBO Mol Med* **5**, 1821-1834, doi:10.1002/emmm.201302654 (2013).

17 Paradisi, A. *et al.* Netrin-1 up-regulation in inflammatory bowel diseases is required for colorectal cancer progression. *Proc Natl Acad Sci U S A* **106**, 17146-17151, doi:10.1073/pnas.0901767106 (2009).

18 Paradisi, A. *et al.* NF-kappaB regulates netrin-1 expression and affects the conditional tumor suppressive activity of the netrin-1 receptors. *Gastroenterology* **135**, 1248-1257, doi:10.1053/j.gastro.2008.06.080 (2008).

19 Fitamant, J. *et al.* Netrin-1 expression confers a selective advantage for tumor cell survival in metastatic breast cancer. *Proc Natl Acad Sci U S A* **105**, 4850-4855, doi:10.1073/pnas.0709810105 (2008).

20 Delloye-Bourgeois, C. *et al.* Netrin-1 acts as a survival factor for aggressive neuroblastoma. *J Exp Med* **206**, 833-847, doi:10.1084/jem.20082299 (2009).

21 Sung, P. J. *et al.* Cancer-Associated Fibroblasts Produce Netrin-1 to Control Cancer Cell Plasticity. *Cancer Res* **79**, 3651-3661, doi:10.1158/0008-5472.CAN-18-2952 (2019).

22 Park, K. W. *et al.* The axonal attractant Netrin-1 is an angiogenic factor. *Proc Natl Acad Sci U S A* **101**, 16210-16215, doi:10.1073/pnas.0405984101 (2004).

23 Arakawa, H. Netrin-1 and its receptors in tumorigenesis. *Nat Rev Cancer* **4**, 978-987, doi:10.1038/nrc1504 (2004).

24 Brisset, M., Grandin, M., Bernet, A., Mehlen, P. & Hollande, F. Dependence receptors: new targets for cancer therapy. *EMBO Mol Med* **13**, e14495, doi:10.15252/emmm.202114495 (2021).

25 Hao, W. *et al.* The pan-cancer landscape of netrin family reveals potential oncogenic biomarkers. *Sci Rep* **10**, 5224, doi:10.1038/s41598-020-62117-5 (2020).

26 Dumartin, L. *et al.* Netrin-1 mediates early events in pancreatic adenocarcinoma progression, acting on tumor and endothelial cells. *Gastroenterology* **138**, 1595-1606, 1606 e1591-1598, doi:10.1053/j.gastro.2009.12.061 (2010).

27 Kefeli, U. *et al.* Netrin-1 in cancer: Potential biomarker and therapeutic target? *Tumour Biol* **39**, 1010428317698388, doi:10.1177/1010428317698388 (2017).

28 Haerinck, J. & Berx, G. Partial EMT takes the lead in cancer metastasis. *Dev Cell* **56**, 3174-3176, doi:10.1016/j.devcel.2021.11.012 (2021).

29 Simeonov, K. P. *et al.* Single-cell lineage tracing of metastatic cancer reveals selection of hybrid EMT states. *Cancer Cell* **39**, 1150-1162 e1159, doi:10.1016/j.ccell.2021.05.005 (2021).

30 Yang, J. *et al.* Guidelines and definitions for research on epithelial-mesenchymal transition. *Nat Rev Mol Cell Biol* **21**, 341-352, doi:10.1038/s41580-020-0237-9 (2020).

31 Jin, X. *et al.* Netrin-1 interference potentiates epithelial-to-mesenchymal transition through the PI3K/AKT pathway under the hypoxic microenvironment conditions of non-small cell lung cancer. *Int J Oncol* **54**, 1457-1465, doi:10.3892/ijo.2019.4716 (2019).

32 Zhang, X. *et al.* Netrin-1 elicits metastatic potential of non-small cell lung carcinoma cell by enhancing cell invasion, migration and vasculogenic mimicry via EMT induction. *Cancer Gene Ther* **25**, 18-26, doi:10.1038/s41417-017-0008-8 (2018).

33 Yan, W. *et al.* Netrin-1 induces epithelial-mesenchymal transition and promotes hepatocellular carcinoma invasiveness. *Dig Dis Sci* **59**, 1213-1221, doi:10.1007/s10620-013-3016-z (2014).

34 Han, P. *et al.* Netrin-1 promotes cell migration and invasion by down-regulation of BVES expression in human hepatocellular carcinoma. *Am J Cancer Res* **5**, 1396-1409 (2015).

35 Revenco, T. *et al.* Context Dependency of Epithelial-to-Mesenchymal Transition for Metastasis. *Cell Rep* **29**, 1458-1468 e1453, doi:10.1016/j.celrep.2019.09.081 (2019).

36 DeConti, R. C. Chemotherapy of squamous cell carcinoma of the skin. *Semin Oncol* **39**, 145-149, doi:10.1053/j.seminoncol.2012.01.002 (2012).

37 Khansur, T. & Kennedy, A. Cisplatin and 5-fluorouracil for advanced locoregional and metastatic squamous cell carcinoma of the skin. *Cancer* **67**, 2030-2032, doi:10.1002/1097-0142(19910415)67:8<2030::aid-cncr2820670803>3.0.co;2-k (1991).

38 Chen, Q. Y. *et al.* miR-206 regulates cisplatin resistance and EMT in human lung adenocarcinoma cells partly by targeting MET. *Oncotarget* **7**, 24510-24526, doi:10.18632/oncotarget.8229 (2016).

39 Liberzon, A. *et al.* The Molecular Signatures Database (MSigDB) hallmark gene set collection. *Cell Syst* **1**, 417-425, doi:10.1016/j.cels.2015.12.004 (2015).

40 Grandin, M. *et al.* Structural Decoding of the Netrin-1/UNC5 Interaction and its Therapeutical Implications in Cancers. *Cancer Cell* **29**, 173-185, doi:10.1016/j.ccell.2016.01.001 (2016).

41 Mak, M. P. *et al.* A Patient-Derived, Pan-Cancer EMT Signature Identifies Global Molecular Alterations and Immune Target Enrichment Following Epithelial-to-Mesenchymal Transition. *Clin Cancer Res* **22**, 609-620, doi:10.1158/1078-0432.CCR-15-0876 (2016).

42 Srinivas, S. *et al.* Cre reporter strains produced by targeted insertion of EYFP and ECFP into the ROSA26 locus. *BMC Dev Biol* **1**, 4, doi:10.1186/1471-213x-1-4 (2001).

43 Barker, N. *et al.* Identification of stem cells in small intestine and colon by marker gene Lgr5. *Nature* **449**, 1003-1007, doi:10.1038/nature06196 (2007).

44 Tuveson, D. A. *et al.* Endogenous oncogenic K-ras(G12D) stimulates proliferation and widespread neoplastic and developmental defects. *Cancer Cell* **5**, 375-387, doi:10.1016/s1535-6108(04)00085-6 (2004).

45 Jonkers, J. *et al.* Synergistic tumor suppressor activity of BRCA2 and p53 in a conditional mouse model for breast cancer. *Nat Genet* **29**, 418-425, doi:10.1038/ng747 (2001).

46 Boussouar, A. *et al.* Netrin-1 and Its Receptor DCC Are Causally Implicated in Melanoma Progression. *Cancer Res* **80**, 747-756, doi:10.1158/0008-5472.CAN-18-1590 (2020).

47 Satija, R., Farrell, J. A., Gennert, D., Schier, A. F. & Regev, A. Spatial reconstruction of single-cell gene expression data. *Nat Biotechnol* **33**, 495-502, doi:10.1038/nbt.3192 (2015).

48 Traag, V. A., Waltman, L. & van Eck, N. J. From Louvain to Leiden: guaranteeing well-connected communities. *Sci Rep* **9**, 5233, doi:10.1038/s41598-019-41695-z (2019).

49 Zappia, L. & Oshlack, A. Clustering trees: a visualization for evaluating clusterings at multiple resolutions. *Gigascience* **7**, doi:10.1093/gigascience/giy083 (2018).

50 Korsunsky, I. *et al.* Fast, sensitive and accurate integration of single-cell data with Harmony. *Nat Methods* **16**, 1289-1296, doi:10.1038/s41592-019-0619-0 (2019).

51 Franzen, O., Gan, L. M. & Bjorkegren, J. L. M. PanglaoDB: a web server for exploration of mouse and human single-cell RNA sequencing data. *Database (Oxford)* **2019**, doi:10.1093/database/baz046 (2019).

52 Buttner, M., Ostner, J., Muller, C. L., Theis, F. J. & Schubert, B. scCODA is a Bayesian model for compositional single-cell data analysis. *Nat Commun* **12**, 6876, doi:10.1038/s41467-021-27150-6 (2021).

53 Elyada, E. *et al.* Cross-Species Single-Cell Analysis of Pancreatic Ductal Adenocarcinoma Reveals Antigen-Presenting Cancer-Associated Fibroblasts. *Cancer Discov* **9**, 1102-1123, doi:10.1158/2159-8290.CD-19-0094 (2019).
54 Trapnell, C. *et al.* The dynamics and regulators of cell fate decisions are revealed by pseudotemporal ordering of single cells. *Nat Biotechnol* **32**, 381-386, doi:10.1038/nbt.2859 (2014).
55 Saelens, W., Cannoodt, R., Todorov, H. & Saeys, Y. A comparison of single-cell trajectory inference methods. *Nat Biotechnol* **37**, 547-554, doi:10.1038/s41587-019-0071-9 (2019).
56 Subramanian, A. *et al.* Gene set enrichment analysis: a knowledge-based approach for interpreting genome-wide expression profiles. *Proc Natl Acad Sci U S A* **102**, 15545-15550, doi:10.1073/pnas.0506580102 (2005).

## METHODS

### *Compliance with ethical regulations.*

Mouse colonies were maintained in a certified animal facility in accordance with the European guidelines. All the experiments were approved by the corresponding ethical committee (Commission d'Etique et du Bien-Être Animal CEBEA, Faculty of Medicine, Université Libre de Bruxelles). CEBEA follows the European Convention for the Protection of Vertebrate Animals used for Experimental and other Scientific Purposes (2010/63/UE). The mice were checked every day and were euthanized when the tumour reaches the end-point size ($2cm^3$) or if the tumour was ulcerated (independently of the size) or if the mouse lost > 20% of its initial weight or showed any other sign of distress (based on general health status and spontaneous activity). None of the experiments performed in this study surpassed the size limit of the tumours. All the experiments complied strictly with the protocols approved by ethical committee. The housing conditions of all animals were strictly following the ethical regulations. The room temperature ranged from 20 and 24°C. The relative ambient humidity at the level of mouse cages was 55 per cent +/-10. Each cage was provided with food, water and two types of

nesting material. Semi-natural light cycle of 12:12 was used. All the experiments complied strictly with the protocols approved by ethical committee.

For subcutaneous grafting using Ishikawa cells, Female Swiss nude mice, 6-weeks old, were purchased from Janvier laboratories (France) and maintained in specific pathogen-free conditions (P-PAC, Lyon, France) and stored in sterilized filter-topped cages. Their care and housing were in accordance with institutional European guidelines as put forth by the CECCAP local Ethical Committee.

***Mouse strains.***

Rosa26-YFP mice[42], Lgr5CreER mice[43], KRasLSL-G12D mice[44] and p53fl/fl mice[45] were imported from the NCI mouse repository and Jackson Laboratories. NOD/SCID/Il2Rγ null mice were purchased from Charles River. All mice used in this study were composed of males and females with mixed genetic background. No randomization and no blinding were performed in this study. tgNTN1 (for hNTN1 gain of function) mice was imported from Mehlen Laboratory – Apoptosis, cancer and development, Centre de Recherche en Cancérologie, Lyon, France[46].

***Lgr5CreER/ Kras$^{LSL\text{-}G12D}$/p53$^{fl/fl}$/Rosa26-YFP$^{+/+}$ (LKPR) and Lgr5CreER/ Kras$^{LSL\text{-}G12D}$/p53$^{fl/fl}$/Rosa26LSL-YFP$^{+/+}$/Rosa26LSL-hNTN1 (LKPRhNTN1) induced skin Squamous Cell Carcinoma (SCC).***

The model Lgr5CreER/ KrasLSL-G12D/p53fl/fl/Rosa26-YFP+/+ (LKPR) is a combination of a crossing of genetically modified mice: Rosa26-YFP mice[42], the Lgr5CreER mice[43], KrasLSL_G12D mice[44] and p53fl/fl4 mice[45] and has been developed in our laboratory[13]. Technically, intraperitoneal administration of Tamoxifen (estrogen analog) (Sigma,

Cat#T5648-1G) activates cre recombinase which is merged to oestrogen ERT2 specifically in hair follicle stem cells expressing Lgr5. Irreversible Cre/Lox recombination bring expression of Kras oncogene, loss of p53 suppressor gene, expression of the YFP reporter gene as tool for lineage tracing of tumour cells. Tamoxifen was diluted at 25 mg/ml in sunflower seed oil, 10% EtOH (Sigma). Four daily intraperitoneal (IP) injections of 2.5 mg tamoxifen were administered at P28 as previously described[13] to LKPR mice. After 7-9 week after Tamoxifen injection tumour appearance and size were detected by daily observation and palpation. Mice were euthanized when tumour size was reached or when mice presented signs of distress (see Compliance with ethical regulations). Skin tumours were measured using a precision calliper. Tumour volumes were measured on the first day of appearance of the tumour and then every week until the death of the animal or every 2 days during chemotherapy assay in combination with Anti-Netrin-1 antibody. To generate the Lgr5CreER/ $Kras^{LSL\text{-}G12D}/p53^{fl/fl}$/Rosa26LSL-$YFP^{+/+}$/Rosa26LSL-hNTN1 (LKPRhNTN1) model which is the LKPR model with overexpression of Netrin-1 in tumour cells, we crossed the Rosa26-Lox-Stop-Lox(LSL)-Netrin-1 transgenic mice. These mice conditionally overexpress flag-tagged Netrin-1 under the control of a Rosa26 promoter[46].

***Cell culture***

FACS isolated EPCAM+ and EPCAM- cells were cultured in Modified eagle medium (MEM) (Capricorn scientific, Cat#SP-2002-500ml) supplemented with 10% Foetal bovine serum (FBS) (Serana, Cat#S-FBS-SA-015), 4µg/ml hydrocortisone (Sigma, Cat#H0888) 1% penicillin/streptomycin (100X) (Capricorn scientific, Cat#PS-B), 2mM L-glutamine, 2ml amphotericin B (100X) (Capricorn scientific, Cat#AMP-B) and 500µl T3 (Sigma, Cat#T6397). Cells were washed with Dulbecco's phosphate buffered saline (PBS 1X) detached from the cell culture plate with trypsin (Capricorn scientific, Cat#TRY-2B10).

The A549, a human non small cell lung cancer cell line, has been donated by Pr Derynck (University of California San Fransisco) and has been used *in vitro* as model in which EMT is plastic and can be induced by TGF-β1[10]. Cells were cultured in DMEM (Gibco, Cat#11965092) with 10% FBS and 1% penicillin/streptavidin. For in EMT induction, cells have been plated, deprived in FBS the day after for 24h, then treated with recombinant TGF-β1 (Peprotech, Cat#100-21) at 5ug/ml *in vitro* for 3 days or 6 days (treatment every 2 days) in DMEM 1.5% FBS.

The Ishikawa cell line, a well-differentiated endometrial adenocarcinoma cell line with Netrin-1 and UNC5B expression, was purchased from the American Type Culture Collection (ATCC). They were grown in Minimum Essential Medium (Ozyme Cat#COR10-009-CV), supplemented with 1% of penicillin/streptomycin and 5% FBS at 37°C with saturating humidity and 5% CO2.

***In vitro invasion assays***

Regarding invasion assays on Ishikawa cell line, experiments were carried out using the xCELLigence RTCA DP instrument (Agilent, Cat#56665817001) which was placed in a humidified incubator at 37°C and 5% CO2. Invasion experiments were performed using 16-well integrated Boyden chamber RTCA CIM plates (ref 5665817001 Agilent). Wells were prepped by depositing 190µl of cell free culture medium (5% FBS) in lower chambers and 20µl of cell free serum free culture medium complemented with 2,5% of Matrigel (Corning) on the porous membranes. CIM plates were placed in the humidified incubator (37°C, 5% CO2) for 1 hour to let the Matrigel polymerize. Ishikawa cells that had been treated with NP137 or its isotypic control NP001 at 20ng/ml for 72h were harvested, suspended in serum free medium, counted, and 150 000 Ishikawa cells were seeded 170µl serum free medium complemented

with NP137 or its isotypic control NP001 at 20ng/ml in the CIM plates upper chambers. CIM plates were then placed in the xCELLigence RTCA DP instrument and cell invasion was monitored by detection of cells passing through the porous membrane and attaching to the impedance microelectrode in the lower chamber.

***In vitro migration assays***

Regarding migration assays with Epcam- cells (Primary LKPR mouse skin SCC cell lines), experiments were carried out using transwell migration plates (6.5 mm Transwell with 8.0 µm, Corning, Cat#3422). Cells had been deprived in FBS (0,5%) for 12h before to be plated in migration plate. Wells were prepped by depositing 150µl of cell culture medium (10% FBS) in lower chambers (control or supplemented with NP137 at 20ug/ml) and 50µl serum free culture medium containing 5 000 cells. Plates were placed in the humidified incubator (37°C, 5% CO2) for 18 hours for migration progression. To detect that had passed through the porous membrane, lower side of transwell has been fixed using fresh PFA 4%, transwells have been washed in PBS and bottom side of transwells had been cleaned. Lower side of membrane have been then stained with 0.2% crystal violet (in 20% methanol) for 20 min. After several washes, passed cells have been counted using reversed microscope.

***Lentiviral transfection/transduction using ShRNA.***

HEK 293T (Human embryonic kidney 293T) (ATCC) were used as packaging cells. Transfer plasmid pLKO.1-puro, carrying our gene of interest *Unc5b* or *Ntn1* (Sigma), TRC1 as empty vector, PPAX and PMDG packaging plasmids were transfected into the cells with lipofectamine 2000 (Thermo Fisher Scientific) using Opti-medium (Capricorn scientific). Cell line of interest (EPCAM+ Primary mouse skin SCC cell lines derived from LKPR) was plated and transduced

with the lentiviral ShRNA with additional polybrene (Sigma, Cat#T2-1003G). Puromycin resistance test has been realized after transduction.

***Anti-Netrin-1 treatment in vivo on primary LKPR mice***

For *in vivo* experiments, to determine the effect of anti-Netrin-1 molecule on primary tumour progression and metastasis, LKPR mice were treated intraperitoneally with anti-Netrin-1 monoclonal antibody at 10 mg/kg every two days from 4 weeks after Tamoxifen injection and until the death of animal (see compliance with ethical regulation part). In combination with chemotherapeutics drugs, the 5-Fluoracil (5-FU) has been used at 10mg/kg and Cisplatin at 4,4mg/kg once a week for 2 weeks and mice were treated with anti-Netrin-1 antibody every two days.

***FACS isolation of tumour cells.***

Skin tumours from *Lgr5CreER/Kras*$^{LSL\text{-}G12D}$*/p53*$^{fl/fl}$*/Rosa26-YFP*$^{+/+}$ mice were dissected, rinsed and digested in collagenase type I (Sigma) at 3,5mg/ml in HBSS (Gibco) for 1h at 37°C on a rocking plate protected from the light. Collagenase was blocked by the addition of EDTA (5mM) and then the cells were rinsed 1 time in PBS supplemented with 10% FBS and the cell suspension were filtered through a 70-µm cell trainer (BD Bioscience). For the wash next and antibody incubation, cells were resuspended in PBS supplemented with 2% FBS (facs buffer). For cell sorting, cells were also filtered through a 40-µm cell trainer (BD Bioscience). Cells were incubated with BV711- conjugated anti-EPCAM (rat, clone G8.8, BD Bioscience Cat#563134, dilution 1:100), PE-conjugated anti-CD45 (rat, clone 30-F11, BD, Cat#553081, dilution 1:100) and PE-conjugated anti-CD31 (rat, clone MEC 13.3, BD, Cat#553373, dilution 1:100) antibodies for 30 min at 4 °C protected from light. Living single tumour cells were selected by forward and side scatter, doublet discrimination and Hoestch exclusion. Tumour

753 cells were selected by YFP expression and the exclusion of CD45 and CD31 ($Lin^-$). Different
754 tumour cell subpopulations were defined in $EPCAM^+$ and $EPCAM^-$ tumour cells. FACS and
755 analysis were performed using FACSAria and LSRFortessa, using FACSDiva software (v.9.1,
756 BD Bioscience). Sorted cells were collected in culture medium complemented with 50% FBS
757 for *in vivo* vein tail injection experiments and generation of culture cell lines or lysis buffer for
758 RNA extraction from RNeasy micro kit (Qiagen).

759 To analyze EPCAM profile on FACS on EPCAM+ LKPR cell line, cells were washed in PBS
760 and detached from the cell culture plate with trypsin. Cells were resuspended and washed with
761 PBS supplemented with 2% FBS (Facs buffer) and incubated with BV711- conjugated anti-
762 EPCAM (rat, clone G8.8, BD Bioscience Cat#563134, dilution 1:200) 30min at room
763 temperature and protected from the light. For cell sorting, cells were washed 2 times in Facs
764 buffer and filtered through a 40-µm cell trainer. Living single YFP+/ EPCAM+ tumour cells
765 were selected by forward and side scatter, doublet discrimination and Hoestch exclusion.
766

767 ***Metastasis assay.***
768 Primary tumours from mice were generated as described above and collected. FACS-isolated
769 tumour EPCAM- cells subpopulation was resuspended in 50 µl PBS and injected into the tail
770 vein of NOD/SCID/Il2Rγ-null mice (1000 cells per injection). Mice were treated with NP137
771 every 2 days (10 mg/kg) for 1 month. Mice were killed after the last treatment and lungs were
772 analysed. The number of metastases was quantified on 10 cryosections per lung (separated by
773 100 µm) based on YFP+ (skin SCCs tumours) expression and presented as number (#) of
774 metastases per lung.
775
776

***Tumour transplantation assays.***

Female Swiss nude mice, 6-weeks old, were purchased from Janvier laboratories (France) and maintained in specific pathogen-free conditions (P-PAC, Lyon, France) and stored in sterilized filter-topped cages. Their care and housing were in accordance with institutional European guidelines as put forth by the CECCAP local Ethical Committee as previously described (C2EA-15, CLB_2014_001; CLB_2014_012; CECCAPP_CLB_2016_017). Animals were subcutaneously injected with Ishikawa cells ($5x10^6$) suspended in 100µL of PBS in the flank. Tumors were allowed to grow for 15 days. Once tumors reached a volume of $100mm^3$, mice were stratified into treatment groups with 1 tumor per mouse based on their tumor volume at the start of the experiment, such that the starting tumor volume in each group were uniform. Mice were treated via intravenous injection of 100µl of NP137 or its isotypic control NP001 diluted in PBS at 20mg/kg for 3 days, then 10mg/kg every 2 days thereafter for 1 month. Tumors were measured every 2 days with calipers. Tumor size was calculated using the formula: tumor volume (mm3) = $(D \times d^2) / 2$ ($mm^3$).

A549 tumour cells have been pre-treated *in vitro* with TGF-β1 for 6 days (see cell culture section) then collected in Matrigel 50% + PBS 50% to be subcutaneously grafted into NOD/SCID mice ($1x10^6$ cells for each grafting point). Secondary tumours were detected by palpation every week and their size were monitored until tumour reach 1 cm or when mice presented signs of distress. The mice were killed at the same time and tumours have been collected for histology analyses.

***Immunofluoresence stainings.***

All stainings were performed on frozen sections. Tumour tissues and lungs were pre-fixed in 4% PFA for 2 h at room temperature, rinsed in PBS, incubated overnight in 30% sucrose at 4

°C and embedded in OCT (Tissue Tek) for cryopreservation. Tissues were cut into 6-µm sections using a CM3050S cryostat (Leica Microsystems GmbH) and rinsed with PBS three times (5 min). Non-specific antibody binding was blocked with 5% horse serum, 1% BSA and 0.2% Triton X-100 for 1 h at room temperature. Primary antibodies were incubated overnight at 4 °C in blocking buffer. Sections were rinsed in PBS three times (5 min) and incubated with secondary antibodies diluted in blocking buffer at 1:400 for 1 h at room temperature. Nuclei were stained with Hoechst (4 mM) and slides were mounted using SafeMount (Labonord). Image acquisition was performed on a Zeiss Axio Imager.M2 fluorescence microscope with a Zeiss Axiocam MRm camera using Axiovision release 4.8 software. Brightness, contrast and picture size were adjusted using Adobe Photoshop.

***Antibodies for immunostaining.***

For Immunofluorescence the following primary antibodies were used: anti-GFP (goat polyclonal, Abcam Cat#ab6673, dilution 1:500), anti-KRT14 (chicken, polyclonal, Thermo Fisher Scientific Cat#MA5-11599, dilution 1:1 000), anti-VIM (rabbit, clone ERP3776 Abcam Cat#ab92547, dilution 1:500), Anti-TROMA/KRT8 (rat, clone 1/28/21, DSHB Cat#AB_531828, dilution 1:1 000), Anti-PDGFRA (rat, clone APA5, ebioscience, Cat#13-1401, dilution 1:500), Anti-CDH1 (mouse, clone 67A4, BD Cat#563570, dilution 1:500) and anti-pan-CK antibody (clone CKAE/1AE3, Dako Belgium, 1:150). The following secondary antibodies were used (dilution 1:400): anti-rabbit, anti-rat, anti- goat, anti-chicken conjugated to rhodamine Red-X (Jackson ImmunoResearch), Cy5 (Jakson ImmunoResearch) or Alexa Fluor-A488 (Invitrogen).

***Immunoblot analysis***.

Subconfluent cells were washed with cold PBS and lysed in a lysis buffer containing SDS. Lysates were sonicated 5x10min using Bioruptor plus (Diagenode Cat#UCD-300) and cellular debris were pelleted by centrifugation (10,000g 15 minutes at 4°C). Protein quantifications were carried out using the Pierce 660nm Protein assay kit (Thermofisher Cat#22662) with a ionic detergent compatibility reagent (Thermofisher Cat#22663) and measured using Bio-Rad iMark microplate. 30 or 40 µg of protein extracts were loaded onto 4-12% SDS-polyacrylamide gels (Thermo) and blotted onto nitrocellulose sheets. The membranes were then blocked with 5% non-fat dried milk + 0,05% BSA for an hour at room temperature and incubated at 4°C overnight with primary antibodies : Anti-NTN1 (rabbit, clone EPR5428, Abcam, Cat#ab126729, dilution 1: 10 000), anti-CDH1 (Mouse, clone 4A2, Cell Signaling Cat#14472, dilution 1:1000), anti-VIM (rabbit, clone ERP3776 Abcam Cat#ab92547, dilution 1:1000) and anti–β-ACTIN (rabbit, Abcam, Cat#ab8227, dilution 1:2000). After three washes with PBS-T, it was followed by incubation 1h incubation with anti-rabbit secondary antibody (anti-Rabbit IgG HRP NA9340V, 1/5 000, Sigma Aldrichfor, cat#Gena9340) at room temperature. After washing in TBS-T, immunoreactive antibody-antigen complexes were visualized with the enhanced chemiluminescence reagents, West Dura or ECL Chemiluminescence System (Pierce). Membranes were imaged using iBright FL1500, Invitrogen.

***In situ hybridization/RNA FISH.***

All stainings were performed on frozen sections or on cytospin. Tumour tissues were pre-fixed in 4% paraformaldehyde for 2 h at room temperature, rinsed in PBS, incubated overnight in 30% sucrose at 4 °C and embedded in OCT (Tissue Tek) for cryopreservation. Cytospin cell culture were generated using CellspinI (Tharmac) (20 000 cells for 1 cytospin). *In situ* protocol

was performed according to the manufacturer instructions (Advanced Cell diagnostics). The following mouse probes were used: Mm-Aqp1 Cat#504741-C2. Mm-Nrp1 Cat#471621, Mm-Aqp5 Cat#430021-C2, Mm-Vim Cat#457961-C2 or Mm-Krt14 Cat#422521-C3. The LSM-780 (Carl Zeiss) confocal system and ZEN2012 software were used to acquire and analyse the ISH images.

***Bulk RNA sequencing.***

RNA quality was evaluated by Bioanalyzer 2100 (Agilent) prior sequencing. Indexed cDNA libraries were obtained using Ovation Solo RNA-seq Systems (NuGen) according to manufacturer's recommendations. The multiplexed libraries (11 pM/18 pM) were loaded onto flow cells and sequences were produced using a HiSeq PE Cluster Kit v4 and TruSeq SBS Kit v3-HS (250 cycles) on a Novaseq 6000 (Illumina). Approximately 20 million paired-end reads per sample were generated and quality checks were performed with FastQC https://www.bioinformatics.babraham.ac.uk/projects/fastqc/. The adaptor sequences and low-quality regions were trimmed by Trimmomatic. Trimmed reads were mapped against the mouse reference genome (Grcm38/mm10) using STAR software to generate read alignments. Duplicated reads are removed by picard MarkDuplicates. Annotations for Grcm38.87 were obtained from ftp://ftp.ensembl.org/. After transcript assembly, gene level counts were obtained using HTseq and normalized to 20 million of aligned reads. Average expression for each gene in the different sample was computed using two biological replicates and fold changes were calculated between control sample (Empty vector) and sample of interest (*Ntn1* KD or *Unc5b* KD). Genes for which all the mean expressions across the sample were lower than 100 read per million mapped reads were considered not expressed and removed from further analysis. Genes having a fold change of expression greater than or equal to 2 were considered up-regulated and those having a fold change of expression lower than or equal to 0.5 were considered down-

regulated.

***RNA extraction and real-time PCR.***

RNA was extracted from FACS-isolated cells or culture cell lines using RNeasy micro kit (QIAGEN) according to the manufacturer's recommendations. For real-time PCR, after mRNA quantification using Nanodrop1000, the first-strand cDNA was synthesized using Superscript II (Invitrogen) and random hexamers (Roche) in 50 µl final volume. Control of genomic contamination was measured for each sample by performing the same procedure with or without reverse transcriptase. Quantitative PCR assays were performed using 1 ng cDNA as template, SYBRGreen mix (Applied Bioscience) on a Light Cycler 96 (Roche) real-time PCR system. m*Tbp or hHprt* housekeeping genes were used for normalization. The following probes were used : m*Ntn1* Fw – gcaagctgaagatgaacatga, m*Ntn1* Rv – ctttgtcggccttcaggat, m*Unc5b* Fw – ttccagctgcacacaacg, m*Unc5b* Rv – gcagagcagagagcatcca, m*Tbp* Fw tgtaccgcagcttcaaaatattgtat– , m*Tbp* Rv – aaatcaacgcagttgtccgtg, h*NTN1* Fw - aaaagtactgcaagaaggactatgc , h*NTN1* Rv – ccctgcttatacacggagatg, h*CDH1* Fw – cccgggacaacgtttatt, h*CDH1*– Rv gctggctcaagtcaaagtcc, h*HOOK1* Fw – tgctgctgagattatgccagtgga, h*HOOK1* Rv - tcagcctctgctcagtttccagtz, h*MUC1* Fw - gccaggatctgtggtggtaca at, h*MUC1* Rv – tgtctccaggtcgtggacattgat, h*HPRT* Fw – tgaccttgatttattttgcatacc, h*HPRT* Rv - cgagcaagacgttcagtcct

***Single-cell transcriptomic data analysis.***

***Single cell RNA library preparation* and gene expression analysis.**

After FACS isolation, living cells from fresh LKPR control and anti-Netrin-1 treated skin SCC tumours were sorted and loaded onto each channel of the Chromium Single Cell 3' microfluidic chips (V2-chemistry, 10X Genomics) and individually barcoded with a 10X Chromium

controller according to the manufacturer's recommendations (10X Genomics). RNA from the barcoded cells was reverse transcribed, followed by amplification. The libraries were prepared using the Chromium Single Cell 3' Library Kit (V2-chemistry, 10X Genomics), quantified using a low coverage Illumina NextSeq 550 run and sequenced on an Illumina NovaSeq. CellRanger (v3.0.2) was used with the default parameters to demultiplex, align, and annotate the obtained sequencing reads with the 10x Genomics mm10-3.0.0 reference dataset extended with the *Yfp* transgene. The Seurat R package was used to perform further downstream analysis of the gene expression matrices for the treated and control samples separately[47] (v3.1.5). Only cells passing the following criteria were considered for further analysis: between 600 and 8000 uniquely expressed genes and less than 25% of the UMI counts mapping to mitochondrial sequences. For the treated samples (NP137 1 and NP137 2), respectively, 16.926 of the 19.288 cells and 14.104 of 17.620 passed quality control. While for the control samples (Control 1 and Control 2), respectively, 10986 of the 12.180 cells and 5248 of the 8327 cells were considered for downstream analysis.

**scRNA-seq clustering leading to cell types.**

Default parameters of Seurat were used, unless mentioned otherwise. Before determining the cell-cycle state, the read counts were log-normalized and scaled. The scaled expression data for the 2000 most highly variable genes (HVG) (identified using Seurat's FindVariableGenes function) served as input for principal component analysis (PCA). Following that, the JackStraw methodology implemented in Seurat was used to determine the number of significant principal components (PCs) for Leiden clustering[48] and UMAP dimensionality reduction (maximum of 30 PCs). Clustering resolutions ranging from 0.1-1.0 with steps of 0.1, were assessed for stability with the clustree[49] R package (v0.4.2). The lowest stable resolution was

chosen for a general overview of the cell types present in both conditions (control: 0.1 & treated: 0.2). Following that, the Wilcoxon rank-sum was used to identify marker genes for each subcluster, only reporting genes that were expressed in at least 25% of the cells in the cluster and had an average log-fold change of at least 0.25. Batch integration was performed per condition using Harmony[50] (v1.0) with standard parameters. Cell type clusters were subsequently annotated using Seurat's module scoring function and cell type specific marker genes obtained from the PanglaoDB[51] database (version of 27/03/2020). Our annotations were further confirmed by plotting the expression of canonical cell markers as *Ptprc* for immune cells, *Pecam* for endothelial cells, *Cd3d* for T cells and *Col6a3* for CAFs. The clusters containing the tumour cells were characterised by expression of the *Yfp* transgene. Afterwards the two datasets, except for the tumor cells, were integrated using Harmony with 30 PCs and standard parameters/ Leiden clustering was subsequently performed in steps of 0.1 for resolutions ranging from 0.1 to 1.0. The clustree R package was then used to determine the lowest stable resolution (0.2). Cell type clusters were then annotated in the same way as previously described. To compare the abundance of the identified cell types between the control and treated conditions, we used the scCODA algorithm[52]implemented in the pertpy v4.0 Python package using the pericytes as the reference cell type and a false discovery rate (FDR) threshold of 0.2.

**scRNA-seq clustering leading to cell subtypes for CAFs.**

After being rescaled, the combined CAFS cluster across the conditions was further subclustered by using the top 2000 HVG as input for PCA analysis. The number of significant PCs for clustering and UMAP calculation, which ranged from 1 to 30, was determined using the JackStraw methodology. Seurat's AddModuleScore was then used to identify clusters with a high enrichment of PanglaoDB-derived marker genes for other cell types using a resolution

of 0.4 for the Leiden clustering. Following the removal of these clusters, the previous analysis steps were repeated, and stable clustering resolutions for the treated condition were determined using clustree. A resolution of 0.3 was used for the identification of the final CAF subclusters. Harmony was used with standard parameters to perform batch integration. The mouse MSigDB hallmark gene sets and the AUCell R package (v1.8.0). were used to calculate pathway activities. Clusters were assigned the apCAF, iCAF or myCAF label using Seurat's AddModuleScore function and the signatures obtained from Elyada et al.[53] Compositional analysis between the control and treated condition was performed with the scCODA algorithm, implemented in the pertpy v4.0 Python package using the "glycolytic CAFS" as the reference and a FDR threshold of 0.2.

**scRNA-seq clustering leading to EMT states for *Yfp* positive cells and pseudotime analysis.**

For both conditions, all Yfp positive cells (defined as at least having two transcripts assigned to the Yfp transgene) were subclustered. The top 2000 variable genes were used as input for PCA analysis after the counts were rescaled. The JackStraw methodology was then used to calculate the number of significant PCs in a range of 1 to 30. The lowest stable clustering resolution per condition was determined using clustree (control: 0.1, treated: 0.3). Based on PanglaoDB-derived marker genes, the AddModuleScore was used to score clusters that showed an enrichment of expression signatures related to other cell types. Following the removal of these clusters, the preceding steps were repeated, with clustering resolutions of 0.7 and 0.6 used for the control and treated conditions, respectively. Subsequently the obtained clusters were scored as epithelial (*Epcam*+, *Krt14*+, *Vim*-), early hybrid (*Epcam*-, *Krt14*+, *Vim*+), late hybrid (*Epcam*-, *Krt14*- , *Krt8*+, *Vim*+, *Pdgfra*-) or full EMT (*Epcam*-, *Krt14*-, *Krt8*-, *Vim*+, *Pdgfra*+)

based on the expression of *Epcam*, *Krt14*, *Krt8*, *Vim*, *Pdgfra*. The mouse MSigDB hallmark gene sets and the AUCell R package[39] (v1.8.0). were used to analyse pathway activities. Before performing the Wilcoxon rank-sum test with Bonferroni correction for multiple testing between conditions, the area under the curve (AUC) distributions were normalised per sample using linear regression. To compare the abundance of the identified cell subtypes and cell cycle distribution per EMT state between the control and treated conditions, the scCODA algorithm of the pertpy v4.0 Python package was used with the early hybrid EMT state as reference a FDR threshold of 0.2. Harmony with standard parameters was used for batch integration per condition. Pseudotime ordering of YFP positive cells in the G1 cell-phase was calculated using monocle[54] (v2.14.0) with the DDRtree (v0.1.5) method for dimensionality reduction on the top 2000 HVGs for each condition, controlling for sample effects. The dynplot[55] R-package (v1.0.2) was used to create the trajectory plots.

***Visium spatial transcriptomic analysis***.

To analyze the spatial distribution and localization of different EMT tumors states previously described by scRNA-seq in Control and anti-Netrin-1 treated skin SCC tumors, we used 10x VISIUM technology for spatial transcriptomic analysis (10X Genomics). FFPE tissue section were places on Visium slides and prepared according to 10x Genomics protocols. After H&E staining, imaging and decrosslinking steps, tissue sections were incubated with human specific probes targeting 10,551 genes (10x genomics, Visium Mouse Transcriptome probe Set v1.0). Probes hybridized on mRNA were captures onto Visium slides and gene Expression library were prepared following the provided protocole and sequences on an illumina Novaseq 6000 with 50.000 reads per spot targeted sequencing depth. For each FFPE section, FASTQ files and histology images were processed using 10X Space Ranger v2.0 to obtain matrix associated to

each spots. SCutility method was used to perform the analysis. Briefly, filtered matrix were loaded, merged per sample and spot with less than 1000 detected genes were removed.

***EMT score***

Three signatures were used to assess the EMT level. The "Hallmark" signature was computed using ssGSEA[56] on the genes from the "HALLMARK_EPITHELIAL_MESENCHYMAL_TRANSITION" signature, as obtained from MSigDB[39] while the "Thiery" signature was computed similarly using the genes from[12]. The "Mak" signature was calculated from the gene sets in PMID: 26420858, as the difference of two signatures: a mesenchymal signature defined as the mean of the mesenchymal genes expressions and an epithelial signature defined as the mean of the epithelial genes expressions.

***Statistical analysis.***

All statistical analyses are based on biological replicates (n indicated in the text, figures or figure legends). Multiple unpaired t-test were performed using graphPad Prism version 9.00 for Mac software. Bar graphs and dot plots were generating with mean +s.e.m by graphPad Prism. Wilcoxon rank-sum test and Fisher test with Bonferroni correction have been used for multiple analyses in single cell RNA sequencing.

**Extended data Figure Legends**

**Extended data 1. Strategy to study the impact of Netrin-1 on EMT in mouse skin SCCs.** **a,** Mouse model of skin SCC allowing the expression of *Kras*$^{G12D}$, *YFP*, *p53* deletion and overexpression of human NETRIN-1 in hair follicle stem cells and their progeny using *Lgr5CreER*. **b,** Relative mRNA expression of *Ntn1* in EPCAM- control (n= 5) and NETRIN-1 gain of function (n= 8) skin SCC defined by qRT-PCR (data are normalized to *Tbp* gene, mean ± s.e.m., two tailed Mann-Whitney U test). **c**, Western blot analysis of Netrin-1 expression in EPCAM- control and NETRIN-1 gain of function skin SCC TCs. **d**, FACS plots showing the gating strategy used to FACS-isolate or to analyse the proportion of YFP$^{+}$/EPCAM$^{+}$ and EPCAM$^{-}$ tumour cells. **e**, Drawing showing the experimental strategy of NP137 administration after Tamoxifen induction in *Lgr5CreER/Kras*$^{LSL\text{-}G12D}$*/p53*$^{fl/fl}$*/Rosa26-YFP*$^{+/+}$ mice. IP, intraperitoneal.

**Extended data 2. Single cell analysis of the cellular composition of control and NP137-treated skin SCCs. a, b** Uniform Manifold Approximation and Projection **(**UMAP) plot for control (**a**) and NP137 -treated skin SCC (**b**) coloured by the identified cell types. **c**, **d**, UMAP plot for control (c) and NP137-treated skin SCC (d) coloured by the sample of origin for each cell. CAFs, cancer-associated fibroblasts.

**Extended data 3. Annotation of the cell types found by single cell RNA-seq in control and NP137-treated skin SCCs. a,** UMAP plots coloured by normalized *Yfp* and *Epcam* expression in the control tumours. Gene expression values are visualized as colour gradient with grey indicating no expression and red indicating the maximum expression. **b**, UMAP plots coloured by normalized *Yfp* and *Epcam* in NP137- treated samples. **c,** UMAP plots coloured by the

activity of modules containing the mouse-specific marker genes of the different cell types including CAFs, Macrophages, Neutrophils, Endothelial cells and T cells obtained from the PanglaoDB database in control samples (left) and anti-Netrin-1 treated samples (right). Module activity visualized as a colour gradient with blue indicating no expression and yellow indicating maximum activity. **d**, UMAP plots coloured by normalized *Pdgfra*, *Acta2*, *Pecam1*, *Cd3d*, *Ptprc*, *Itgam*, *Cd86* and *Cxcr2* expression in the control samples (left) and NP137- treated samples (right). CAFs, cancer-associated fibroblasts. **e**, UMAP plot coloured by normalized *Ntn1* expression in control condition.

**Extended data 4. Impact of anti-Netrin antibody administration on the cellular composition of skin SCCs. a**, **b**, Uniform Manifold Approximation and Projection (UMAP) plots coloured by the cell type labels obtained from the analysis of the microenvironment for the integration of all the samples in total and split per sample, respectively. **c,** Boxplot depicting the proportions of the different cell types for the 4 samples, split by their condition. The boxplots are coloured by their condition, and the individual measurements are visualized as red dots. The centre line, top and bottom of the boxplots represent respectively the median, 25th and 75th percentile and whiskers are 1.5 × IQR. Significant proportion changes are indicated by FDR < 0.2. **d,** barplot depicting the relative log fold change of the relative abundance of the different cell types after NP137-treated samples compared to the pericytes. Bars are coloured according to their cell type. **e, f,** UMAP plot of the CAFS subclustering, coloured by the identified seven subclusters and the sample the cell originated from, respectively. **g,** Boxplot depicting the proportions of the different CAF subclusters for the 4 samples, split by their condition. The boxplots are coloured by their condition, and the individual measurements are visualized as red dots. The centre line, top and bottom of the boxplots represent respectively the median, 25th and 75th percentile and whiskers are 1.5 × IQR. **h.** barplot depicting the

relative log fold change of the relative abundance of the different CAF subclusters after NP137-treatment compared to the glycolysis CAFs subcluster. **i**, Co-immunostaining of YFP and Vimentin in control (top) (n= 5 tumours) and NP137- treated skin SCC (bottom) (n= 5 tumours) that defines YFP-/VIM+ CAFs as cells (Scale bars, 20 μm).

**Extended data 5. Expression of markers of the different EMT states in control and NP137-treated skin SCCs. a, b**, UMAP plots coloured by normalized gene expression values for the indicated genes in the control (**a**) and treated samples (**b**). Gene expression values are visualized as colour gradient with grey indicating no expression and red indicating the maximum expression. Circles represent TCs groups with a different degree of EMT based on the expression of *Epcam*, *Krt14*, *Krt8*, *Vim*, *Pdgfra* (green: *Epcam+/Krt14+/Vim-* as epithelial state; orange: *Epcam-/Krt14+/Vim+* as early hybrid EMT state; red: *Epcam-/Krt14-/Krt8+/Vim+* as late hybrid EMT state; dark red: *Epcam-/Krt14-/Krt8-/Vim+* as late full EMT state expressing *Pdgfra* and *Aqp1*). **c**, Barplot depicting the relative log fold change of the relative abundance of the different EMT states after NP137-treatment compared to the early hybrid state. Significant proportion changes are indicated by FDR < 0.2.

**Extended data 6. Histological analysis of the control and NP137-treated tumors. a-d, .** Haematoxylin and Eosin staining showing the control (n=1) (**a**, **b**) or NP137-treated (n=1) (**c**, **d**) tumour skin SCC analysed in Visium spatial transcriptomic method. The annotated areas represent the EMT states previously defined by the expression of *Epcam*, *Krt14*, *Krt8* and *Vim* (1: epithelial, 2: early hybrid, 3, late hybrid, 4: full late EMT) (scale bars in a, c, 500 μm, scale bars in b, 20 μm)**.**

**Extended data 7. Analysis of NP137 treatment on tumour growth, EMT and migration in endometrial human cancer cell line. a,** Tumor growth quantification of human Ishikawa

endometrial carcinoma cells grafted in nude mice treated with either control (n=9) or NP137 (n=9) (mean ± s.e.m., 2-way ANOVA). **b**, Relative mRNA expression of epithelial markers *CDH1*, *MUC1* and *HOOK1* by qRT-PCR in Ishikawa human cells grafted in nude mice treated with control (n=7) or NP137 (n=8) (data are normalized to *HPRT* gene, mean +/- s.e.m., two tailed Mann-Whitney U test). **c**, Percentage of migrated Ishikawa cells treated with NP137 relative to the migration of control condition through serum deprived culture medium complemented with 2.5% Matrigel between 5 and 24 hours of invasion. (n=3) (mean ± s.e.m, two tailed t test).

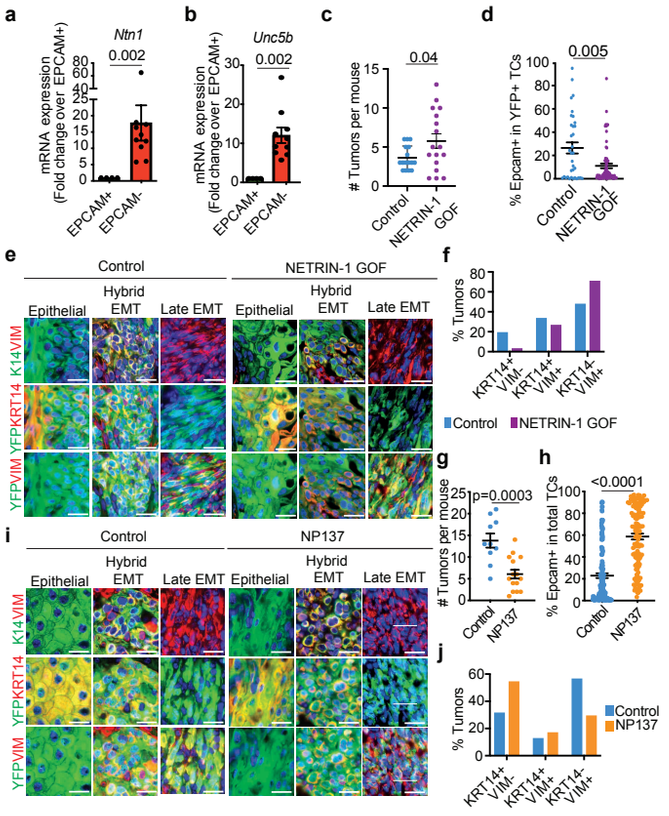


**Lengrand et al Fig. 1**

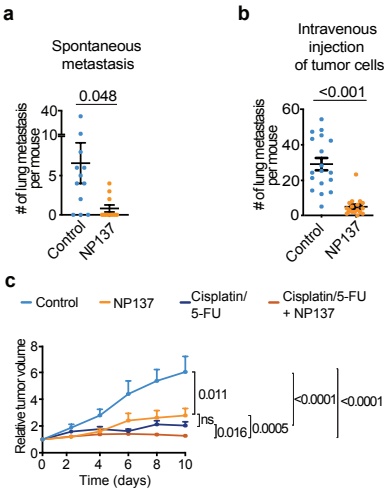


**Lengrand et al Fig. 2**

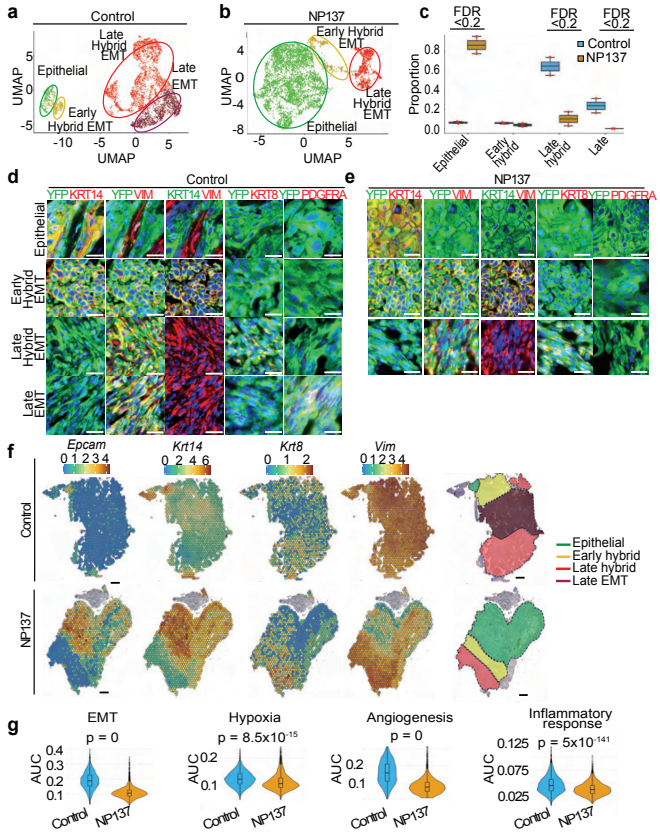


**Lengrand et al Fig. 3**

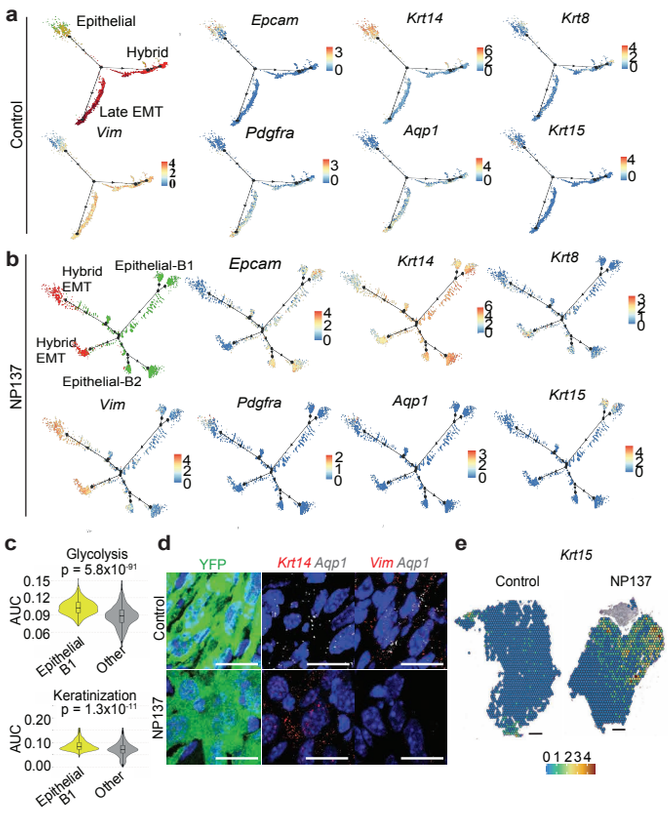


**Lengrand et al Fig. 4**

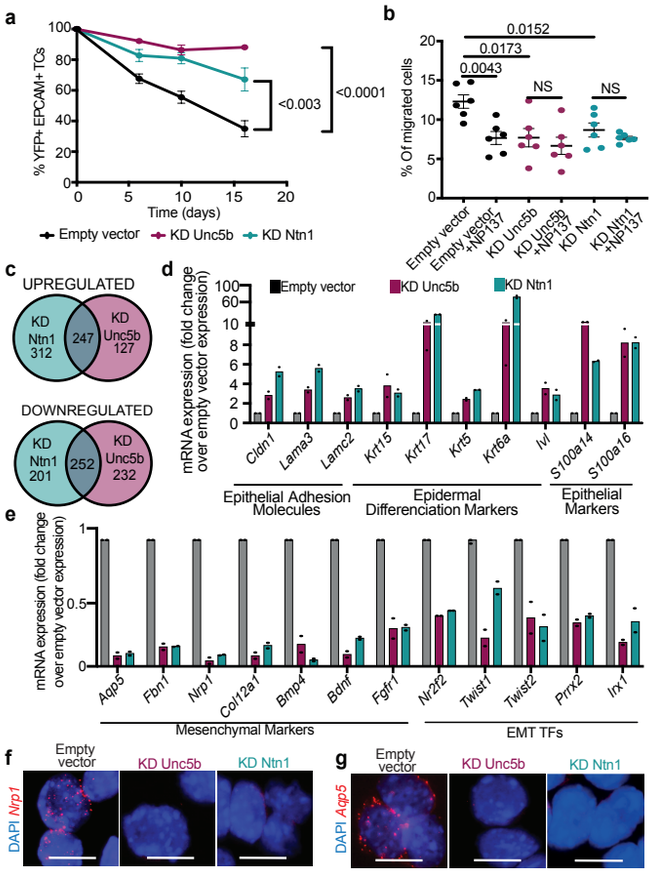


**Lengrand et al Fig. 5**

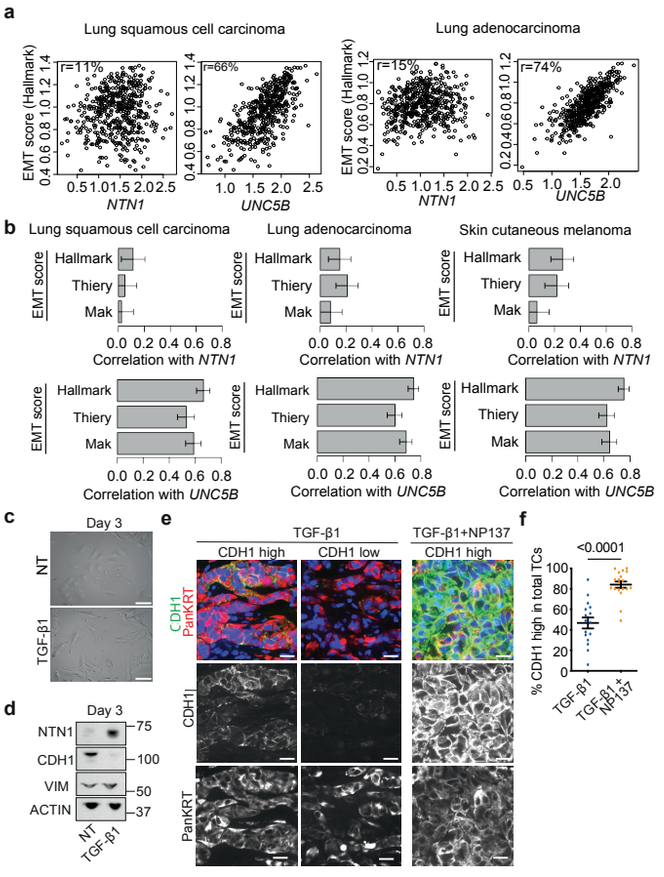


**Lengrand et al Fig. 6**